Fluid Instability in MHD Shocks due to Cosmic Ray Pressure Gradients

Philip Mocz
Astronomy 253
Harvard University

April 21, 2014

Abstract

We investigate magnetic field amplification in a magnetohydrodynamic (MHD) shock caused by a cosmic ray (CR) pressure gradient acting on the inhomogeneous medium upstream of the shock. We write a publicly-available numerical MHD solver[1] in MATLAB to solve the MHD equations coupled to an advecting and diffusing CR pressure fluid quantity. The method uses a finite volume approach with a constrained transport scheme for the magnetic fields, and use the Crank-Nicolson implicit 2nd-order method to solve the advection-diffusion equation of the CR fluid. This approximate treatment of CRs makes it easy to be included in large cosmological simulations in future work, where a shock finder could be used to inject a source of CR pressure. The simulations demonstrate that a CR pressure gradient upstream generates turbulence though differential acceleration which in turn amplifies pre-existing magnetic fields considerably, making it possible to have much larger magnetic fields upstream in the shock than estimated via jump conditions. We explore the dependence of the instability on variations in the initial conditions of the density perturbations, extending the investigated parameter space of previous work, and find that it is possible to excite the instability and obtain the same level of amplification even if there is little power in small-scale density perturbations initially in the upstream. Detailed Faraday rotation measurements of this instability could be used to infer the upstream density inhomogeneities in supernova shocks and cluster outskirts.

Key words: magnetic fields – (magnetohydrodynamics) MHD – plasmas – cosmic rays – instabilities – methods: numerical

1 Introduction

Both theoretical arguments and observational evidence suggest that magnetic fields may be substantially amplified by CRs in strong shock conditions in certain astrophysical systems

[1] available at: `https://bitbucket.org/pmocz/crmhd`

such as supernova remnants. A number of theoretical arguments claim a variety of instabilities may exist in the plasma which amplifies the magnetic field, and is supported by indirect observational evidence from Vink & Laming (2003); Berezhko *et al.* (2003); Bamba *et al.* (2004, 2005); Völk *et al.* (2005); Ballet (2006); Parizot *et al.* (2006); Vink (2012); Uchiyama *et al.* (2007); Yamazaki *et al.* (2004). Strong magnetic fields (larger than what is expected from just adiabatic compression) are needed to explain the acceleration of CR particles up to the high energies at which they are observed.

One important identified instability is the Bell mechanism. The work by Bell (2004) points out that strong current-driven instability might be present in remnants. Current is carried by non-magnetized high-energy CR particles, driving a return current in the thermal plasma. However, this process can only generate fields on scales smaller than the gyro-radius of the driving particles. Additional processes such as inverse cascades may be necessary to process the magnetic fields on large enough scales so that they are able to accelerate the highest energy particles that are observed.

An alternate mechanism is proposed by Beresnyak *et al.* (2009). In this mechanism, CR pressure drives small-scale dynamo action which amplifies the pre-shock magnetic field. This mechanism works on much larger scales and produces significant amplification. This is the instability which we investigate in this work.

The said CR pressure instability was first studied numerically by Drury & Downes (2012), who made a simple 2D simulation of an MHD fluid (just upstream the shock) with density fluctuations and a constant pressure gradient. The work was recently extended by another group, Brüggen (2013), by self-consistently coupling the CR pressure to the MHD equations using an isotropic diffusion and advection. In this paper, we investigate the instability via simulations using the later formulation. We investigate in greater detail the dependence of the instability on variations in the initial conditions of density inhomogeneities in the upstream in a perpendicular magnetic field shock.

This instability may be present in more than just supernova remnants. Observations suggest that magnetic field amplification takes place in the weak shocks in galaxy clusters that produce "radio relics" (100s kpc scale diffuse synchrotron sources in galaxy clusters caused by shocks from major mergers propagating through the intra-cluster medium) (Markevitch *et al.*, 2005; van Weeren *et al.*, 2011). Diffusive shock (or Fermi-I) acceleration is present in these shocks, just as in the supernova remnants, but the observed magnetic fields far upstream the shock are too weak to accelerate particles up to the highest energy levels observed. Amplification of the magnetic fields upstream the shock by the CR pressure instability may play an important role in these systems.

This instability may potentially exist in solar flares as well, given there exist density inhomogeneities in the upstream of a strong shock.

The structure of the paper is organized as follows. In § 2 we present the physical, analytic picture for the reason of the instability. In § 3 we describe the numerical method we used. In § 4 we describe the simulation setup. In § 5 we present and discuss the results of the simulations, demonstrating the amplification by the instability and exploring the power spectrum and other characteristics of the resulting turbulence. Finally, in § 6 we offer concluding remarks.

2 Physical Basis

The physics of the instability is described in the present section (the argument is due to Drury & Downes (2012)). The setup is the following. Suppose the incoming flow upstream the shock has density perturbations $\delta\rho$ on a length scale λ (i.e., the gas is "clumpy" as would be the case in a turbulent medium), and that there is a CR pressure gradient upstream the shock (due to diffused CRs). The density fluctuations operate on order of the advection time through the precursor. Then, this will lead to velocity fluctuations (on the same length scale λ) on order of:

$$\delta v \sim \frac{\delta\rho}{\rho_0}\frac{F_{\rm cr}}{\rho_0}\frac{D}{v_{\rm up}} \tag{1}$$

where $F_{\rm cr}$ is the magnitude of the force per unit volume due to the CR pressure gradient: $\mathbf{F}_{\rm cr} = -\nabla P_{\rm C}$, D is the diffusion coefficient for the CR pressure, ρ_0 is the background average density, and $v_{\rm up}$ is the upstream velocity.

In order for turbulence to develop, the eddy turn-over time ($\frac{\lambda}{\delta v}$) has to be short compared to the outer scale ($\frac{L}{v_{\rm up}}$), which implies the not-very restrictive condition that:

$$\frac{\lambda}{\delta v} \ll \frac{D}{v_{\rm up}^2} \tag{2}$$

The magnetic field is amplified in the usual stretch-fold manner by the solenoidal component of the velocity field in the precursor.

3 Numerical Method

We solve the MHD equations coupled to an isotropic CR pressure fluid quantity (this formalism may also be extended to non-isotropic CR pressure). In hyperbolic conservation form, the equations are written as:

$$\frac{\partial \mathbf{U}}{\partial t} + \nabla \cdot \mathbf{F} = \mathbf{S} \tag{3}$$

where $\mathbf{U}$ is the vector of the conserved variables, $\mathbf{F}(\mathbf{U})$ is the flux, and $\mathbf{S}$ are source terms, namely:

$$\mathbf{U} = \begin{pmatrix} \rho \\ \rho\mathbf{v} \\ \rho e \\ \mathbf{B} \end{pmatrix}, \quad \mathbf{F}(\mathbf{U}) = \begin{pmatrix} \rho\mathbf{v} \\ \rho\mathbf{v}\mathbf{v}^T + p - \mathbf{B}\mathbf{B}^T \\ \rho e\mathbf{v} + p\mathbf{v} - \mathbf{B}(\mathbf{v}\cdot\mathbf{B}) \\ \mathbf{B}\mathbf{v}^T - \mathbf{v}\mathbf{B}^T \end{pmatrix}, \quad \mathbf{S} = \begin{pmatrix} 0 \\ \mathbf{F}_{\rm cr} \\ \mathbf{F}_{\rm cr}\cdot\mathbf{v} \\ 0 \\ 0 \end{pmatrix}, \tag{4}$$

where $p = p_{\rm gas} + \frac{1}{2}\mathbf{B}^2$ is the total gas pressure, $e = u + \frac{1}{2}\mathbf{v}^2 + \frac{1}{2\rho}\mathbf{B}^2$ is the total energy per unit mass, u is the thermal energy per unit mass. The equation of state for the fluid is given by $p = (\gamma - 1)\rho u$. We use an adiabatic index of $\gamma = 5/3$. $\mathbf{F}_{\rm cr}$ is the force per volume due to the CR pressure gradient, given by:

$$\mathbf{F}_{\rm cr} = -\nabla P_{\rm C} \tag{5}$$

The CR pressure $P_{\rm C}$ is evolved according to an advection-diffusion equation:

$$\frac{\partial P_{\rm C}}{\partial t} + \nabla \cdot (P_{\rm C}\mathbf{v}) = \nabla \cdot (D \nabla P_{\rm C}) \tag{6}$$

where D is the diffusion coefficient. CRs are injected by enforcing at all times that at the location of the shock:

$$P_{\rm C} = \eta \rho_{\rm up} v_{\rm up}^2 \tag{7}$$

where η is an efficiency factor.

The primitive fluid variables ρ, $\mathbf{v}$, P are solved numerically using a standard second-order finite volume Godunov scheme on a fixed Cartesian grid, described in full detail in Mocz *et al.* (2014). The basic idea of a finite volume method is that the domain is discretized into cells, and each cell keeps track of volume-averaged fluid quantities, which are evolved. The evolution step to the next time-step is performed by extrapolating the solution of the primitive fluid variables out to the center of the faces at the middle of the time step and solving the Riemann problem to obtain a flux across the cell faces. This results in a naturally conservative scheme, as whatever fluid quantity leaves one cell enters another. In the case of a solution with shocks, a slope-limiter has to be applied to prevent the solution from oscillating in the presence of strong discontinuities.

The magnetic field $\mathbf{B}$ is updated via a constrained transport (CT) algorithm, due to Evans & Hawley (1988) for solving the MHD equations on a Cartesian grid, and extended to arbitrary unstructured static and moving meshes in Mocz *et al.* (2014). The basic idea of the CT algorithm is to use a discretization of the magnetic field that preserves the $\nabla \cdot \mathbf{B} = 0$ of the MHD equations exactly to machine precision. $\nabla \cdot \mathbf{B} = 0$ is an extra constraint in the MHD equations that is satisfied throughout the entire evolution of the fluid as long as it is satisfied by the initial condition, but it is not needed to evolve the fluid. It is important to keep $\nabla \cdot \mathbf{B}$ near 0 in simulations otherwise the results may be unstable or even unphysical. The key idea in the numerical method is to exploit Stokes' theorem and uses a face-averaged representation of the magnetic fields (called the 'staggered-mesh' approach) to enforce $\nabla \cdot \mathbf{B} = 0$. In the algorithm, the z component of the electric fields are predicted at the cell edges (using an interpolation of the Riemann fluxes) at the middle of the time-step and used to update the magnetic fields of the faces. Cell-averaged magnetic fields may then be computed from the face-averaged magnetic fields.

Finally, the advection-diffusion equation for CR pressure $P_{\rm C}$ has to be solved using a different numerical scheme, since it has both a hyperbolic and a parabolic term. It is advanced in time implicitly (as opposed to explicitly as in the finite volume scheme) using a second-order Crank-Nicolson scheme.

The code is written in MATLAB, and is intended to be a simple, minimal, modular code that can be used as a nice introduction to anyone interested in computational methods for MHD. The code is publicly available at `https://bitbucket.org/pmocz/crmhd`.

4 Simulation Setup

We set a value of $D = 1.0$, but our simulations can be rescaled to other values of D. We also set $\eta = 0.6$. We simulate a 2D planar shock in the frame of the shock. The box has

Simulation	range of k_x,k_y	description
1	$-32:32$	includes small-scale initial density inhomogeneities
2	$-8:8$	does not include small-scale initial density inhomogeneities

size 2×1 and the shock is located in the center of the box at $x = 1$. At the location of the shock, the CR pressure is always enforced to be $\eta \rho_{\rm up} v_{\rm up}$. The upstream is located on the left and the downstream is located on the right.

We simulate a shock with Mach number $M = 100$. The initial conditions are chosen to be: $(\rho, P, v_x)_{\rm up} = (1, 0.00006, 1)$ and $(\rho, P, v_x)_{\rm down} = (3.9988036, 0.7499850, 0.2500750)$. These are conditions given by pure hydrodynamic strong shock jump (Rankine-Hugoniot) conditions. The magnetic field is assumed to be negligible initially (set to point in the perpendicular direction with strength $B_y = 0.001$).

Perturbations in the density field are added to the initial conditions. This is accomplished by defining the function f:

$$f(x, y) = \sum_{k_x, k_y} A_i \sin(2\pi(k_x x + k_y y) + \phi_{k_x, k_y}) \tag{8}$$

where i is the index of a wave-vector $\mathbf{k}$. A_i is an amplitude chosen randomly in the range $[0, 1]$. ϕ_{k_x,k_y} are random phases in the range $[0, 2\pi)$. The density distribution is then given by:

$$\rho(x, y) = e^{\beta f(x,y)} \tag{9}$$

where β is a constant chosen so that the field as an RMS of density fluctuations of 0.2. This setup yields a log-normal distribution for the density distribution which is typical of what would be expected in the case of isothermal turbulence. We simulate two cases of initial conditions: [1] k_x,k_y goes from -32 to 32 (lots of power in small-scale perturbations) and [2] k_x,k_y goes from -8 to 8 (little power in small-scale perturbations), see Table 4.

On the x-boundaries we choose inflow/outflow boundary conditions, and enforce periodic BCs on the top and the bottom of the box. At the start of the simulation, the CR pressure is zero everywhere ($P_{\rm C} = 0$), and the shock position is at the center of the box at $x = 1$. The boundary conditions for the CR fluid are outflowing on all sides. The gas is inflowing on the left of the box at $x = 0$ (with density perturbations flowing into the box) and outflowing on the right of the box at $x = 2$. The density condition at $x = 0$ as a function of time is determined by:

$$\rho(t, x = 0, y) = e^{\beta f(-k_x v_{x,\rm up} t, y)} \tag{10}$$

We use a resolution of 256×512 for our simulations, which should yield near converged results of the instability (Drury & Downes, 2012).

5 Results

Figures 1 and 2 show snapshots of the gas density and magnetic field strength for the two simulated cases: case [1] (contains large k initial upstream density perturbations) and case [2] (does not contain large k initial upstream density perturbations). The fluid flows from left

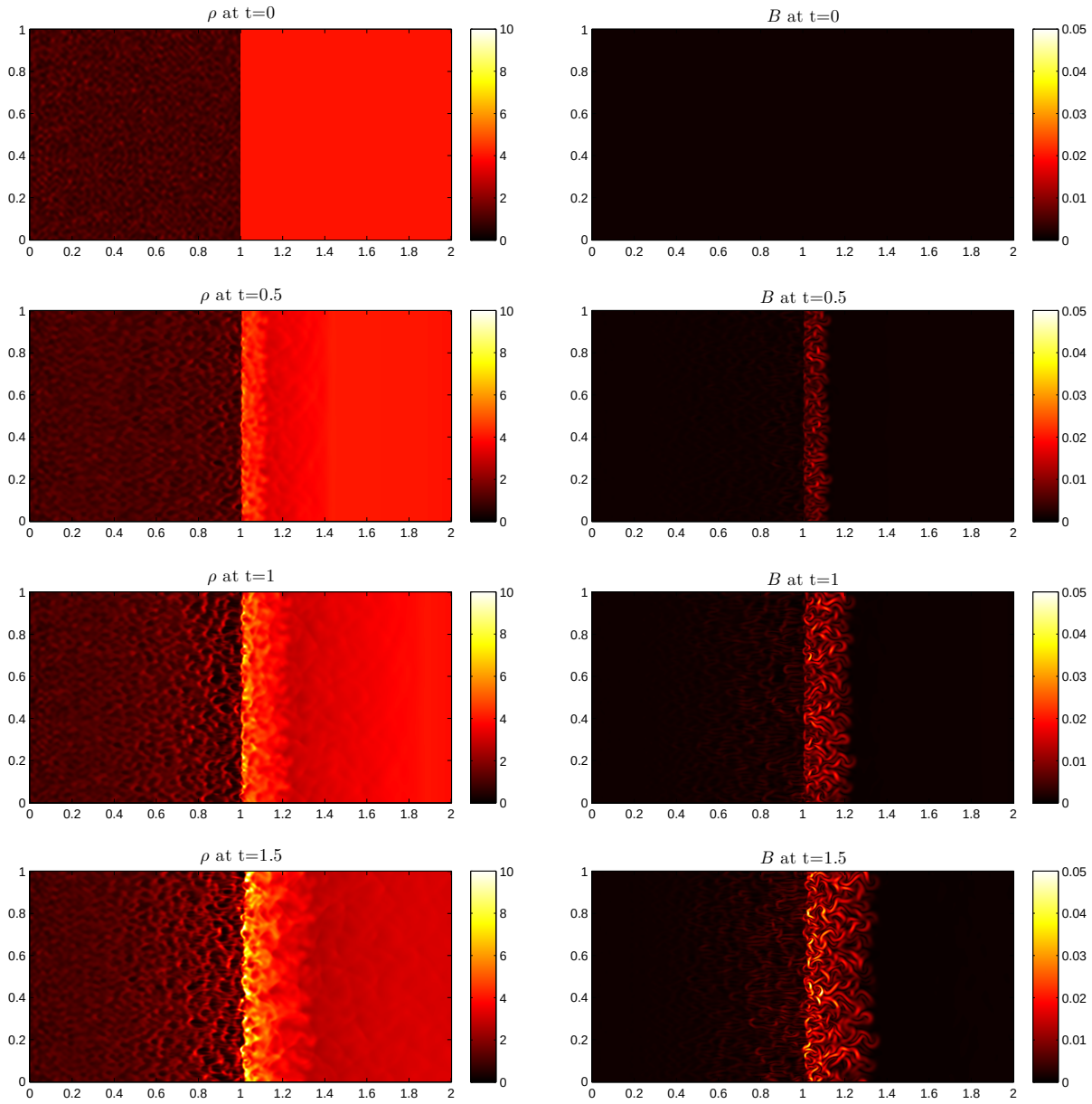

Figure 1: Density and magnetic field strengths in the simulation of case [1].

to right. The left half is upstream of the shock and the right half is downstream. The shock is a strong shock with Mach number $M = 100$ and dynamically-unimportant magnetic fields in the perpendicular (y) direction. The magnetic fields are easily amplified downstream of the shock, due to upstream density inhomogeneities being swept up and processed. By time $t = 1$, it becomes apparent that the upstream also experiences an instability and growth of the magnetic fields. There is an initial linear phase of the instability, followed by a nonlinear phase which leads to saturation of the typical magnetic field strength. The density perturbations become flattened in the upstream and break into smaller pieces. The magnetic fields show amplified regions that are roughly perpendicular to the shock. The size-scale of

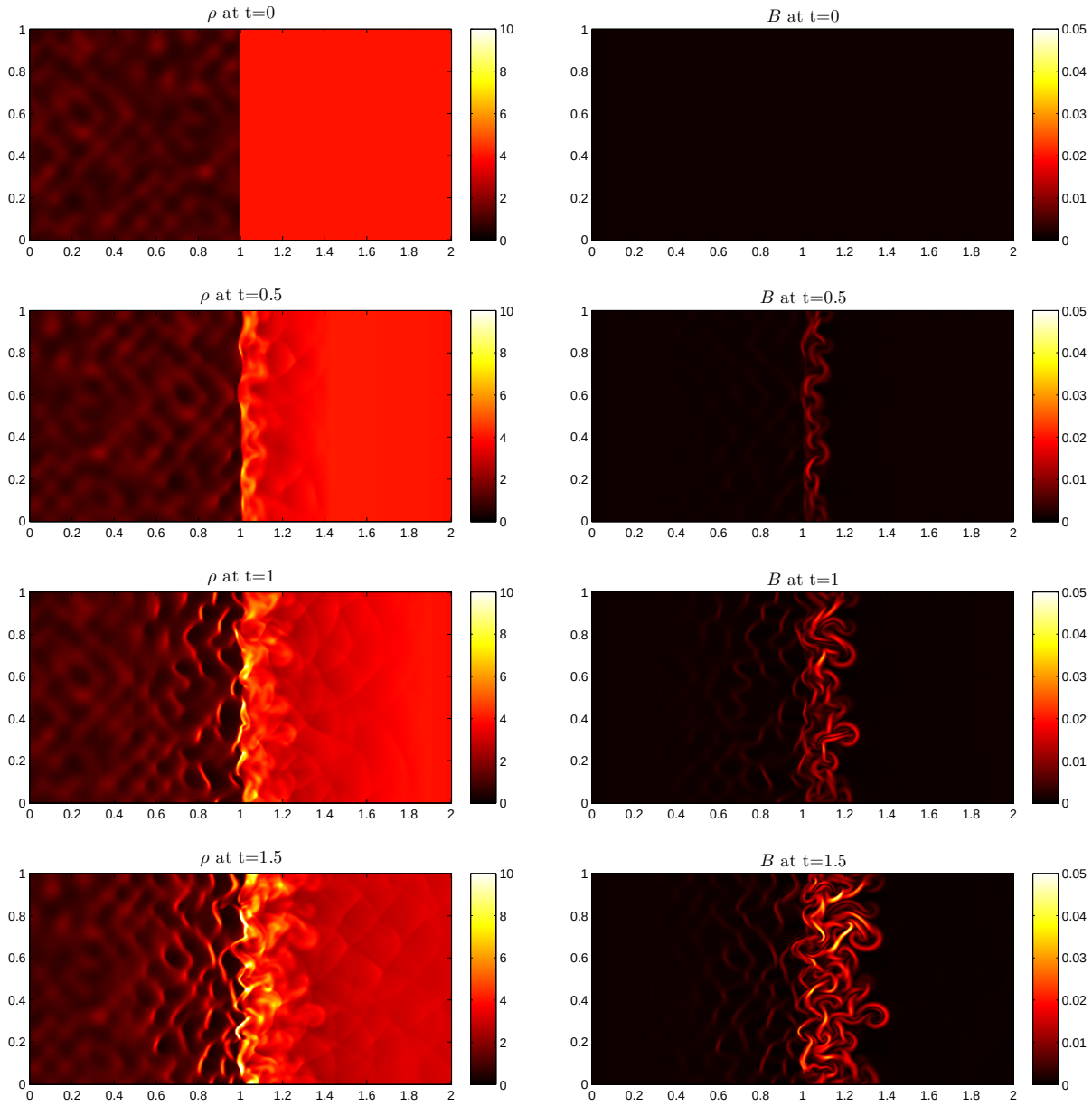

Figure 2: Density and magnetic field strengths in the simulation of case [1].

the density and magnetic field features in the instability are different in the two simulated cases. The features are smaller if we use initial conditions that include small-scale density perturbations. Regardless, the instability develops in both simulations.

In Figure 3 we show the amplification of the magnetic field in the upstream as a function of time for both of the simulated cases. We present the amplification of the density-weighted average magnetic field in the upstream: $\langle B \rangle = \int B\rho\, dV / \int \rho\, dV$, as well as the amplification of the maximal magnetic field as functions of time. The average amplification factor is about 2 in both the simulations (this amplification factor is higher if we choose to average in a domain closer to the shock). One can observe a linear phase and a saturated, non-linear

phase in the amplification. The amplification factor of the maximal magnetic field grows to an order of $20 - 30$, meaning that the magnetic fields can change by more than an order of magnitude due to this simple instability.

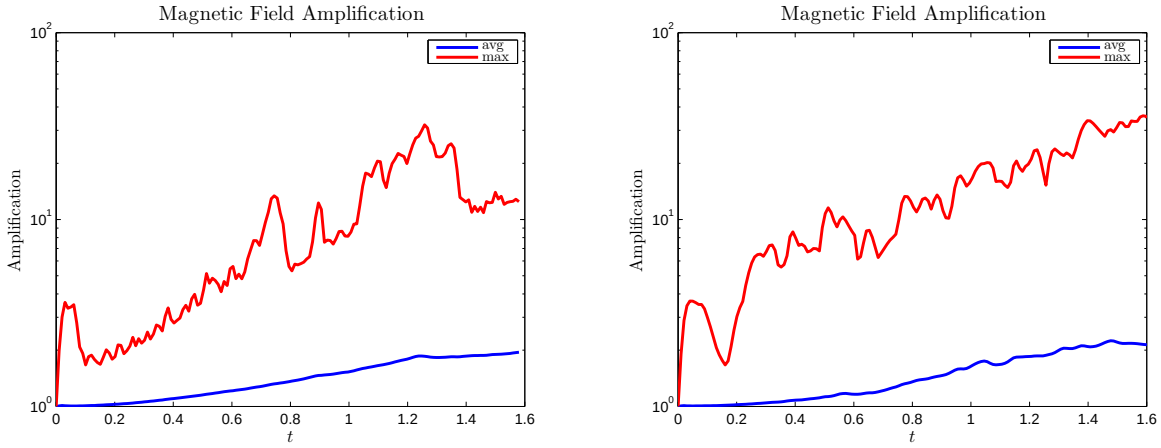

Figure 3: Upstream average and maximal magnetic field amplification (left = case [1], right = case [2])

We present power spectra of the density and magnetic energy density of the upstream in Figure 4. The power spectra peak at $k = 1$ (corresponding to the length of the box) due to periodic boundary conditions. We see that in case [1], the initial density power spectrum has power in the range $k = 1 : 32$, and in case [2] the power is in a more limited range from $k = 1 : 8$. The initial magnetic field is uniform, so there is no power at any k. In both cases, the density power spectra evolves and saturates. In case [1], it gains a characteristic peak at around $k_{\text{peak}} = 11$ and in case [2], it gains a characteristic peak at around $k_{\text{peak}} = 10$. The power spectrum is symmetric about this peak and sustained in time, which is indicative of turbulence. The small physical scale perturbations (large k modes) which do not exist in the initial conditions of case [2] are able to grow very efficiently by this instability. The magnetic field also builds up power on the small scales (large k) due to the instability (with roughly equal power over a range of k's).

In Figure 5 we plot the probability density function (PDF) of plasma density in the upstream for the two simulated cases evolving with time. We see that initially the density has a log-normal PDF, but it quickly evolves to have non-Gaussian tails, with random fluctuations (intermittency) in the lowest and highest density regions. In both simulations, the peak of the PDF shifts to slightly higher densities and converges by $t = 1.5$. There is more low density structure in case [1] and more high density structure in case [2].

In Figure 6 we plot the x-direction velocities at $t = 1.5$ (solution has saturated). We see that the bulk flow upstream decelerates from its initial value as it comes against the CR pressure gradient before it can reach the shock. Different density fluid elements decelerate at different rates, which causes the instability. Very near the shock near the post-shock region, the x component of the velocity may be very close to 0 (in a few cells, the velocity goes very slightly negative), since the magnetic field is strongly amplified here and regions of it point in the y-direction.

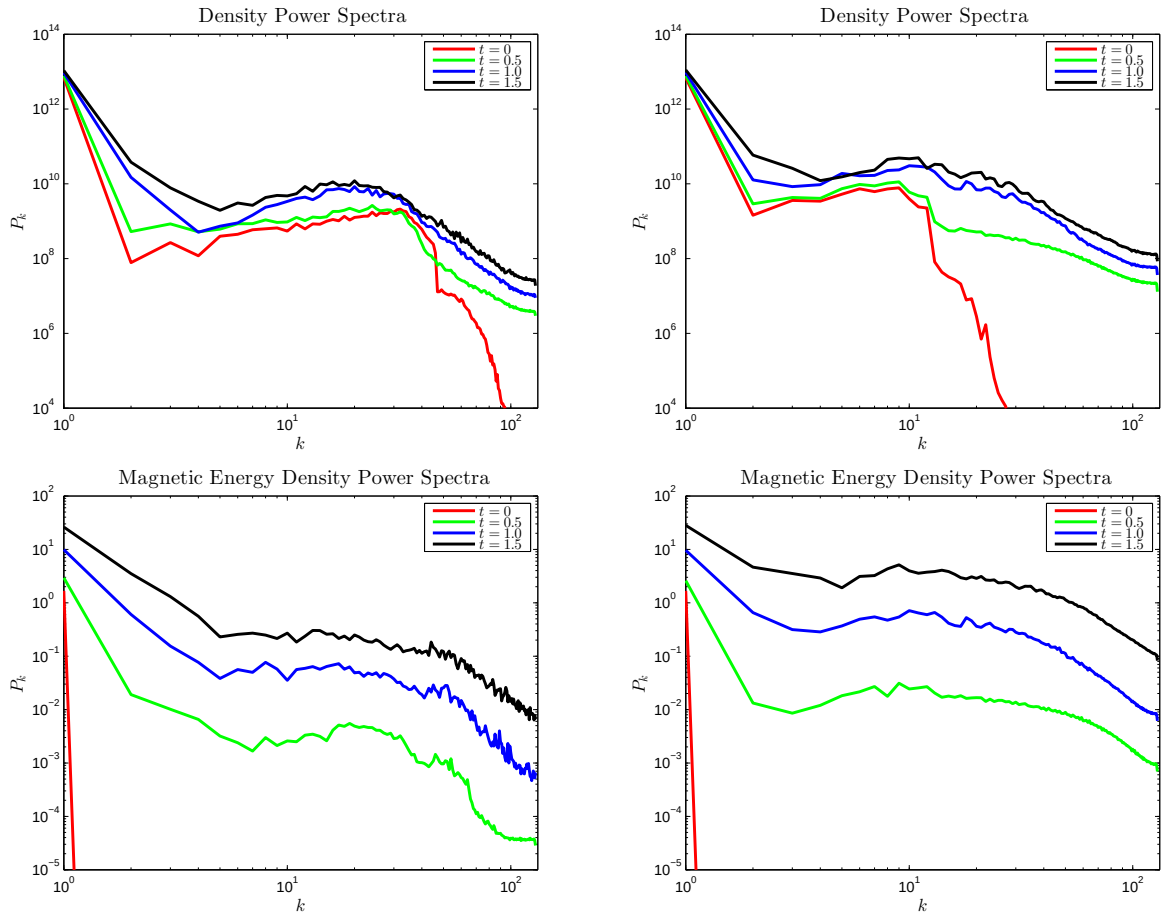

Figure 4: Upstream density and magnetic energy density power spectra in the simulations (left = case [1], right = case [2])

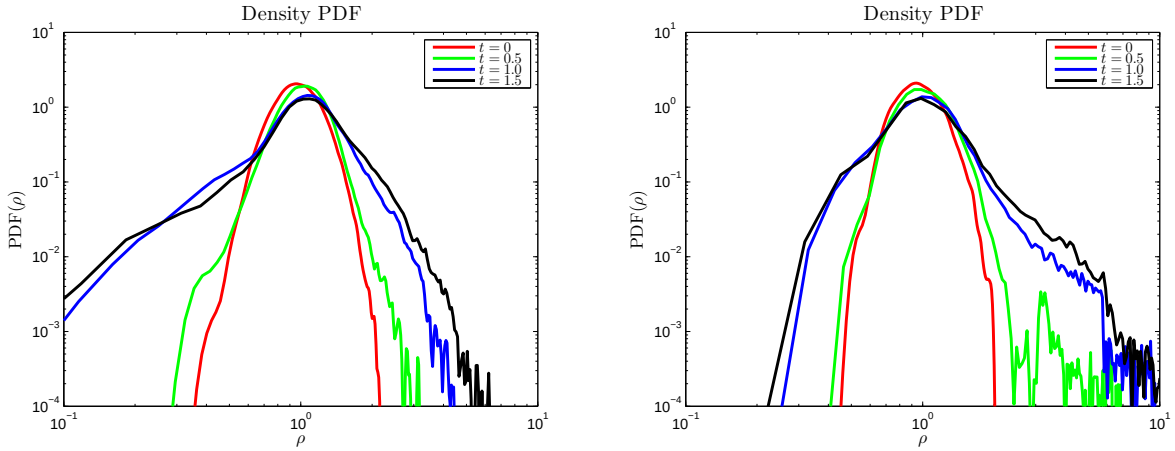

Figure 5: Upstream density PDFs (left = case [1], right = case [2])

Finally, in Figure 7 we show how the typical CR pressure looks like in our simulations. The CR pressure has diffused both upstream and downstream from the shock surface, where

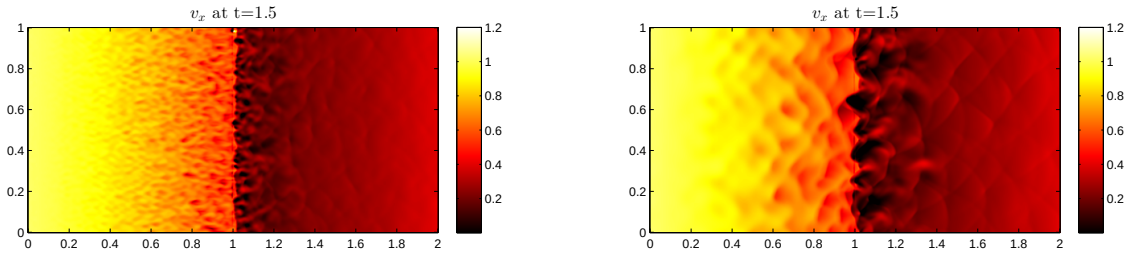

Figure 6: x-direction velocities v_x at $t = 1.5$ (left = case [1], right = case [2])

CR pressure is injected, and has slightly advected towards the right due to the direction of the bulk velocity of the fluid.

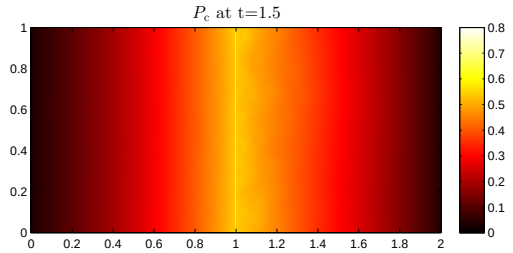

Figure 7: Characteristic profile of the diffused cosmic ray pressure in the simulations.

5.1 Scaling to Physical Parameters

The temporal and spatial coordinates may be normalized by units of $t = D/v_{x,\mathrm{up}}^2$ and $x = D/v_{x,\mathrm{up}}$, and energy densities by units of $\rho v_{x,\mathrm{up}}^2$ (Brüggen, 2013). Then, one can fix a physical unit of length, velocity, and density characteristic of a system, say $L = 100$ kpc, $v = 10^8$ cm s^{-1}, and $\rho = 10^{-26}$ g cm^{-3}. This yields units of energy density of 10^{-1} erg cm^{-1} s^{-2}, and a unit of time of 98 Myr. The diffusion coefficient D may be given by the Bohm diffusion coefficient $D = m_p c^3/(3eB_0) = (3.13 \times 10^{28}\ \mathrm{cm}^2\ \mathrm{s}^{-1})(B/\mu\mathrm{G})^{-1}$.

6 Concluding Remarks

Cosmic-ray pressure amplifies the magnetic fields of shocks, even in the upstream, given density inhomogeneities exist in the fluid. We investigated this instability in a strong shock with Mach number $M = 100$ and weak initial magnetic fields and found that the magnetic fields upstream where amplified by factors up to $20 - 30$ (with an average amplification factor of 2). The same level of amplification was found in two simulations: [1] with initial

upstream density perturbations that include large k modes and [2] without large k modes. We also studied the power spectra of the density and the magnetic energy density and the density PDFs in the upstream to learn more about the shock. We learned that the density profile evolves to peak around a certain $k = k_{\rm peak}$ which is sustained in time, indicative of turbulence. $k_{\rm peak}$ is smaller (i.e. evolved density perturbations are larger-scale) if initially the upstream fluid lacks small scale density perturbations. This would affect the Faraday rotation maps (like the ones constructed by Brüggen (2013)) and could be used as a way to learn information about the clumpiness of the upstream gas. Large k modes are still easily excited even if none exist in the initial conditions. The instability works on the whole range of k's, making it a very important magnetic field amplification mechanism that may operate in supernova remnants and cluster outskirts.

It is important to point out that the instability operates on length scales equal to the length of the precursor (the maximal distance the most energetic CRs diffuse). This length scale is large compared to the gyro-radius, making this instability an easy way to generate large-scale strong magnetic fields. Other instabilities such as the Bell mechanism, which tend to operate on the gryo-radius scale, need some other inverse cascade process to amplify the magnetic field on large scales.

7 Acknowledgments

PM would like to thank Dr. Steven Cranmer and Dr. Nick Murphy for discussing the project topic and providing great lectures on the general subject.

References

Ballet, J. 2006. X-ray synchrotron emission from supernova remnants. *Advances in Space Research*, **37**, 1902–1908.

Bamba, A., Ueno, M., Nakajima, H., & Koyama, K. 2004. Thermal and Nonthermal X-Rays from the Large Magellanic Cloud Superbubble 30 Doradus C. *ApJ*, **602**(Feb.), 257–263.

Bamba, A., Yamazaki, R., Yoshida, T., Terasawa, T., & Koyama, K. 2005. A Spatial and Spectral Study of Nonthermal Filaments in Historical Supernova Remnants: Observational Results with Chandra. *ApJ*, **621**(Mar.), 793–802.

Bell, A. R. 2004. Turbulent amplification of magnetic field and diffusive shock acceleration of cosmic rays. *MNRAS*, **353**(Sept.), 550–558.

Beresnyak, A., Jones, T. W., & Lazarian, A. 2009. Turbulence-Induced Magnetic Fields and Structure of Cosmic Ray Modified Shocks. *ApJ*, **707**(Dec.), 1541–1549.

Berezhko, E. G., Ksenofontov, L. T., & Völk, H. J. 2003. Confirmation of strong magnetic field amplification and nuclear cosmic ray acceleration in SN 1006. *A&A*, **412**(Dec.), L11–L14.

Brüggen, M. 2013. Magnetic field amplification by cosmic ray-driven turbulence - I. Isotropic CR diffusion. *MNRAS*, **436**(Nov.), 294–303.

Drury, L. O., & Downes, T. P. 2012. Turbulent magnetic field amplification driven by cosmic ray pressure gradients. *MNRAS*, **427**(Dec.), 2308–2313.

Evans, C. R., & Hawley, J. F. 1988. Simulation of magnetohydrodynamic flows - A constrained transport method. *ApJ*, **332**(Sept.), 659–677.

Markevitch, M., Govoni, F., Brunetti, G., & Jerius, D. 2005. Bow Shock and Radio Halo in the Merging Cluster A520. *ApJ*, **627**(July), 733–738.

Mocz, P., Vogelsberger, M., & Hernquist, L. 2014. A Constrained Transport Scheme for MHD on Unstructured Static and Moving Meshes. *ArXiv e-prints*, Feb.

Parizot, E., Marcowith, A., Ballet, J., & Gallant, Y. A. 2006. Observational constraints on energetic particle diffusion in young supernovae remnants: amplified magnetic field and maximum energy. *A&A*, **453**(July), 387–395.

Uchiyama, Y., Aharonian, F. A., Tanaka, T., Takahashi, T., & Maeda, Y. 2007. Extremely fast acceleration of cosmic rays in a supernova remnant. *NAT*, **449**(Oct.), 576–578.

van Weeren, R. J., Brüggen, M., Röttgering, H. J. A., & Hoeft, M. 2011. Using double radio relics to constrain galaxy cluster mergers: a model of double radio relics in CIZA J2242.8+5301. *MNRAS*, **418**(Nov.), 230–243.

Vink, J. 2012. Supernova remnants: the X-ray perspective. *AAPR*, **20**(Dec.), 49.

Vink, J., & Laming, J. M. 2003. On the Magnetic Fields and Particle Acceleration in Cassiopeia A. *ApJ*, **584**(Feb.), 758–769.

Völk, H. J., Berezhko, E. G., & Ksenofontov, L. T. 2005. Magnetic field amplification in Tycho and other shell-type supernova remnants. *A&A*, **433**(Apr.), 229–240.

Yamazaki, R., Yoshida, T., Terasawa, T., Bamba, A., & Koyama, K. 2004. Constraints on the diffusive shock acceleration from the nonthermal X-ray thin shells in SN 1006 NE rim . *A&A*, **416**(Mar.), 595–602.